



# Towards ground-to-space radiative closure in the mid- to far-infrared

Benedict Pery<sup>1</sup>, Helen Brindley<sup>1,2</sup>, Jonathan Murray<sup>1,2</sup>, Sophie Mosselmans<sup>1</sup>, Sanjeevani Panditharatne<sup>3</sup>, Laura Warwick<sup>4</sup>, Robin Hogan<sup>3</sup>, Yi Huang<sup>5</sup>, Benjamin Riot–Bret cher<sup>5</sup>, Hilke Oetjen<sup>4</sup>, Dirk Schuettemeyer<sup>4</sup>, and Tristan L’Ecuyer<sup>6</sup>

<sup>1</sup>Department of Physics, Imperial College London, UK

<sup>2</sup>National Centre for Earth Observation, Imperial College London, UK

<sup>3</sup>European Centre for Medium-Range Weather Forecasts, Reading, UK

<sup>4</sup>ESA/ESTEC, Noordwijk, the Netherlands

<sup>5</sup>Department of Atmospheric and Oceanic Sciences, McGill University, Canada

<sup>6</sup>Space Science and Engineering Center, University of Wisconsin-Madison, USA

**Correspondence:** Benedict Pery (b.pery24@imperial.ac.uk)

**Abstract.** Despite containing up to half of the Earth’s thermal emission to space, the far-infrared spectral region (FIR, defined here as  $100\text{--}667\text{ cm}^{-1}$  or  $15\text{--}100\text{ }\mu\text{m}$ ) has seldom been observed from satellites. This has contributed to substantial uncertainties in the spectroscopy of water vapour, radiative properties of clouds, and surface spectral emissivity; these in turn limit confidence in modelled FIR energy flows. With the advent of the Polar Radiant Energy in the Far-InfraRed Experiment (5 PREFIRE), a step is taken towards new, systematic, spectral observations of the Earth in the FIR. Launched in 2024, the two PREFIRE CubeSats offer a new perspective of Earth’s outgoing longwave energy with moderate spectral resolution. However, the observational uncertainty budget requires further consolidation.

In this study we assess the accuracy of PREFIRE spectral measurements through a ‘ground-to-space’ closure experiment. Using zenith-viewing observations from the ground-based Far INfrarEd Spectrometer for Surface Emissivity (FINESSE), we gauge the representativity of atmospheric data from in situ sensors and reanalysis. With these data we simulate PREFIRE-observed radiances for an overflight of our field site in eastern Canada. Simulations of the FINESSE radiances are in very good agreement with observations, while those from PREFIRE indicate some bias beyond the calculated uncertainties. We find that atmospheric water vapour specification, uncertain surface properties, and instrument noise dominate the uncertainties. Based on these findings, we highlight proposed techniques for closure experiments using terrestrial and satellite instruments alike. 15 Such experiments will provide a ground-truth for validation of future FIR satellite missions.

## 1 Introduction

The interaction of thermal infrared radiation with Earth’s atmosphere and surface plays a fundamental role in shaping the planet’s weather and climate. Spectral observations in the thermal infrared can be used to retrieve atmospheric composition and temperature structure, and to understand the complex physics behind Earth system processes. Satellite observations additionally



20 offer a powerful global view of these phenomena, and have been used for decades in the service of meteorology and atmospheric science.

The far-infrared (FIR), defined here as the region from  $100\text{--}667\text{ cm}^{-1}$  (or  $15\text{--}100\text{ }\mu\text{m}$ ) comprises around half of the globally averaged longwave emission to space (Harries et al., 2008), and as such is a crucial component of the Earth's radiation budget. Water vapour is a key atmospheric absorber in the FIR, contributing to the significant FIR greenhouse effect (e.g. Sinha and  
25 Harries, 1995; Brindley and Harries, 1998). Conversely, in very dry and cloudless atmospheric conditions micro-windows 'open' in the FIR. These micro-windows comprise the FIR 'dirty window' region (here defined as  $400\text{--}600\text{ cm}^{-1}$ ), and permit radiation from the surface to escape to space. In this way, surface temperature and emissivity can also affect FIR measurements from space, as well as the top-of-atmosphere energy budget.

Ice clouds exert a strong influence in the FIR, with theoretical studies demonstrating substantial sensitivity of FIR radiances  
30 to the size and shape of ice crystals (Yang et al., 2003; Baran, 2007). More recent analyses using ground- and aircraft-based observations have confirmed this sensitivity and suggest that the region could provide uniquely powerful constraints on retrieved cloud properties (Maestri et al., 2014; Panditharatne et al., 2025; Di Natale et al., 2026).

Nevertheless, the scarcity of FIR observations (relative to other spectral regions such as the mid-infrared and microwave) means that significant uncertainties persist in fundamental gas spectroscopy (e.g. Mlawer et al., 2019), underlying ice optical  
35 properties and hence cirrus radiative properties (e.g. Wang et al., 2024; Bantges et al., 2020), and surface emissivity (e.g. Chen et al., 2014). These uncertainties can propagate into simulations of the future climate (e.g. Turner et al., 2012; Huang et al., 2018).

Despite its scientific importance, spectrally resolved observations of the FIR from satellites have been impeded by limitations of optical and sensor technology. The only such measurements until recently were from a sparse set of missions in the early  
40 satellite era (Hanel et al., 1971; Kempe et al., 1980). However, the launch of the Polar Radiant Energy in the Far-InfraRed Experiment (PREFIRE, L'Ecuyer et al., 2021) in 2024 marks the first step towards filling this FIR observational gap. This mission features two CubeSats launched as part of NASA's Earth Ventures initiative. A relatively low-cost mission, PREFIRE provides moderately resolved spectral radiances stretching into the FIR and aims to contribute to polar science at a time of rapid change in the polar climate. The radiances are used to retrieve temperature, water vapour, surface spectral emissivity, and  
45 spectral fluxes in clear-sky polar scenes, but a first step towards being confident in the accuracy of these retrievals is to have confidence in the radiances themselves.

Unbridled by the stringent requirements of a space mission, a limited set of accurate ground- and aircraft-based instruments observing the FIR has been available for some time. These instruments have furthered knowledge of the FIR radiative properties of several components of the Earth system, including water vapour (e.g. Mlawer et al., 2019) and the surface emissivity  
50 (Bellisario et al., 2017; Murray et al., 2020). Zenith-pointing observations in clear sky have been used to profile the atmosphere with high accuracy, investigate downwelling radiance, and perform closure tests in the FIR (e.g. Mariani et al., 2012; Belotti et al., 2023; Mosselmans et al., 2026).

With the above in mind, in this work we carry out a radiative closure study in clear sky across the mid- to far-infrared, with a focus on the FIR. We use the FINESSE ground-based spectrometer (Murray et al., 2024) to assess the representativity



55 of atmospheric profiles gathered from reanalysis and in situ measurement. The high spectral resolution, accuracy, and known calibration of this spectrometer give us confidence in the accuracy of the atmospheric profiles and of our radiative transfer simulations. We then go on to compare simulations and measurements of satellite radiances from an overpass of the ground measurement site, serving to validate spectral radiance observations from PREFIRE and identify potential instrument biases. As far as we are aware, this work represents the first attempt to perform such an experiment in the far-infrared.

60 The layout of this paper is as follows. The data sources and methods used in the experiment are presented in Sect. 2. In Sect. 3, we discuss the various challenges to a rigorous radiative closure diagnosis, and present a detailed investigation into the sources of uncertainty in the experiment. We present results of the closure experiment, both on the ground and in space, in Sect. 4 and discuss the findings in Sect. 5.

## 2 Data sources and methods

### 65 2.1 The WHAFFERS campaign

The W-band, HiSRAMS, AERI, FIRR2, FINESSE and FIRMOS Experiment on Remote Sensing (WHAFFERS) campaign was a multi-modal field study conducted in Canada, with sites in Ottawa and near Montreal, in January and February of 2025. Observations of the atmosphere and land surface were gathered simultaneously by passive and active instruments across the two sites and from an aircraft. Among the aims of the campaign was to investigate consistencies between radiometric instruments  
70 by performing radiative closure experiments. We investigate a closure experiment in this work with a focus on measurements from the research station at the Gault Nature Reserve of McGill University (45.535° N, 73.149° W). This site sits at c.130 m above sea level on the side of a forested hill, surrounded by mostly flat agricultural land at c.30 m above sea level.

Meteorological conditions were anomalously cold and dry in this region of Canada during the campaign which was ideal for study of the far-infrared. The reduced optical depth of the atmospheric column in the FIR water vapour absorption features  
75 affords greater sensitivity than normal to higher altitudes and to water vapour spectroscopy when measured from the ground.

### 2.2 Spectral measurements

#### 2.2.1 FINESSE

The Far-infrared Spectrometer for Surface Emissivity (FINESSE, Murray et al., 2024) is a ground-based radiometer developed at Imperial College, employing a commercial Bruker EM27 Fourier-transform spectrometer. FINESSE was originally config-  
80 ured to measure over the range 400–1600 cm<sup>-1</sup> with a spectral resolution reaching 0.5 cm<sup>-1</sup>. It features a custom front-end optics system that enables both the study of surface emissivity and zenith-looking views of the atmosphere. FINESSE has been used to retrieve surface emissivity under laboratory conditions (Warwick et al., 2024) and in the field (Warwick et al., 2025) using measurements from a campaign in Andøya, Norway in 2023. Measurements from this field campaign have also enabled study of the polar atmosphere (Mosselmans et al., 2026). The instrument is equipped with ancillary sensors to measure  
85 temperature, pressure, relative humidity, and CO<sub>2</sub> concentration.



Work has been ongoing since the Norway campaign to improve the FINESSE instrument. Replacing the liquid nitrogen cooling with a Stirling cooler has eliminated the need to interrupt measurements and extended the measurement range slightly further into the FIR, now reaching  $380\text{ cm}^{-1}$ . Vibrations induced by the Stirling cooler were removed outside of the required modulated frequency band by doubling the FINESSE scan speed, with each interferometer scan lasting 0.75 s rather than the 1.5 s of the original configuration. Intercomparison with a co-located AERI spectrometer during the WHAFFERS campaign enabled the diagnosis and removal of a small bias between  $1400\text{--}1600\text{ cm}^{-1}$ . This bias was caused by internal reflections in the spectrometer assembly and had gone undetected in the Andøya FINESSE measurements.

### 2.2.2 PREFIRE

The Polar Radiant Energy in the Far-Infrared Experiment mission (PREFIRE, L'Ecuyer et al., 2021) consists of two 6U Cube-Sats in different near-polar Sun-synchronous orbits, each equipped with a Thermal Infrared Spectrometer (TIRS) instrument; the satellites were launched in May/June 2024. The TIRS is a lightweight grating spectrometer covering a spectral range of  $5\text{--}54\text{ }\mu\text{m}$  ( $185\text{--}2000\text{ cm}^{-1}$ ), with a nominal spectral sampling of  $\sim 0.84\text{ }\mu\text{m}$  (equivalent to  $\sim 5\text{ cm}^{-1}$  at  $250\text{ cm}^{-1}$ , or  $\sim 20\text{ cm}^{-1}$  at  $500\text{ cm}^{-1}$ ). The four order sorting filters used in the TIRS instrument split the measurements into four distinct spectral bands. In order of increasing wavelength, these bands are referred to as MIR-1, MIR-2, FIR-1, and FIR-2.

The TIRS grating separates incoming radiation from eight cross-track 'scenes' onto the uncooled detector array, where each scene has a full complement of detectors for all spectral channels. This results in different sensor noise characteristics for each cross-track view. On the Earth's surface, the scenes are non-contiguous and stretch across a 264 km swath, acting as an eight-toothed 'comb' moving along the satellite track. Each field of view (FOV) has a surface footprint of approx  $11.8\times 34.8\text{ km}$  (cross-  $\times$  along-track) with cross-track gaps between of approx 24.2 km. There is substantial overlap in the FOVs in the along-track direction, with any point along the orbit observed by up to 7 overlapping footprints. Note that these values will change as the satellites' orbits decay over the mission lifetime. A single spectrum of the TIRS instrument is recorded at each FOV.

In the initial release (R01) of the PREFIRE level 1 radiance product (1B-RAD), the science team have identified discrepancies between the instrument model of the spectral response functions and the true instrument response. The second release (R02) of the L1B data includes an empirical correction factor for the spectral radiance. This correction can be added to the reported spectral radiance to account for these discrepancies, as is done for the analysis in this study. Figure 1 illustrates the effect of this correction on the spectra used in this study. The correction factor is derived using a combination of three distinct reference radiances: IASI collocated spectra convolved to PREFIRE channels, CrIS collocated spectra convolved to PREFIRE channels, and PCRTM modelled clear-sky radiances derived using the PREFIRE Auxiliary Meteorology product (Mattingly et al., 2025) as input. More details on this correction factor will be published in due course.

### 2.2.3 Selection of spectral data

FINESSE operated on 20 days across the WHAFFERS campaign, collecting approximately 135 hours of measurements. During the FINESSE observation periods, PREFIRE FOVs with valid spectra passed close to (within  $\sim 25\text{ km}$  of) the site on 7 occasions. A further 19 overpasses were not captured by FINESSE due to either the time of the overpass (in the evening or

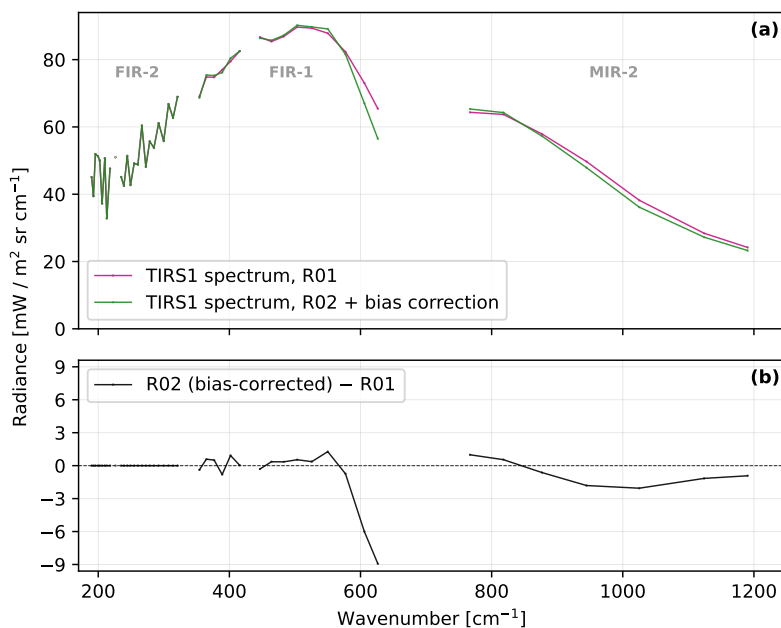


**Figure 1.** (a): Example PREFIRE TIRS 1 spectra (from across-track scene 6) for the first and second release (R01 and R02) of the Level 1 radiance product. The R02 spectrum includes the new bias correction term. Grey text labels the spectral bands of the TIRS instrument. (b): Spectral differences between the two releases.

at night) or weather conditions (FINESSE cannot operate during precipitation). Of the 7 captured, we focus on the PREFIRE  
 120 satellite 1 overpass on 28th January 2025 at 20:52 UTC (15:52 local time). This case was the only one of these 7 to have  
 verifiable clear skies throughout the observed scene and a radiosonde release at the time of the overpass.

For this study we average all spectra from a five minute window of the FINESSE measurements, centred on the PREFIRE  
 overpass. FINESSE was continuously recording in zenith view mode and collected 400 interferometer scans in this time. The  
 spectra exhibit good stability over the measurement period, indicating no marked evolution in the atmospheric state. PREFIRE  
 125 measurements are taken from the Level 1B-RAD product, version R02, with the bias correction factor included. Valid spectra  
 from the overpass whose FOV midpoint was within  $0.25^\circ$  (latitude/longitude) of the Gault station are averaged along-track to  
 yield two spectra for comparison, from the cross-track TIRS 1 scenes 5 and 6. All channels in the MIR-1 PREFIRE band have  
 known calibration issues and so are neglected here.

### 2.3 Ancillary atmosphere and surface data

130 To model infrared radiative transfer in clear skies (that is, neglecting the contributions of cloud and aerosol), we require tem-  
 perature and gas concentrations as functions of pressure or altitude. In the thermal infrared region we study here, encompassing  
 $185\text{--}1600 \text{ cm}^{-1}$  across both instruments, the dominant absorbing and emitting species are water vapour, carbon dioxide, and  
 ozone, with other trace gases such as methane and nitrous oxide also required to simulate spectral radiance with high accuracy.

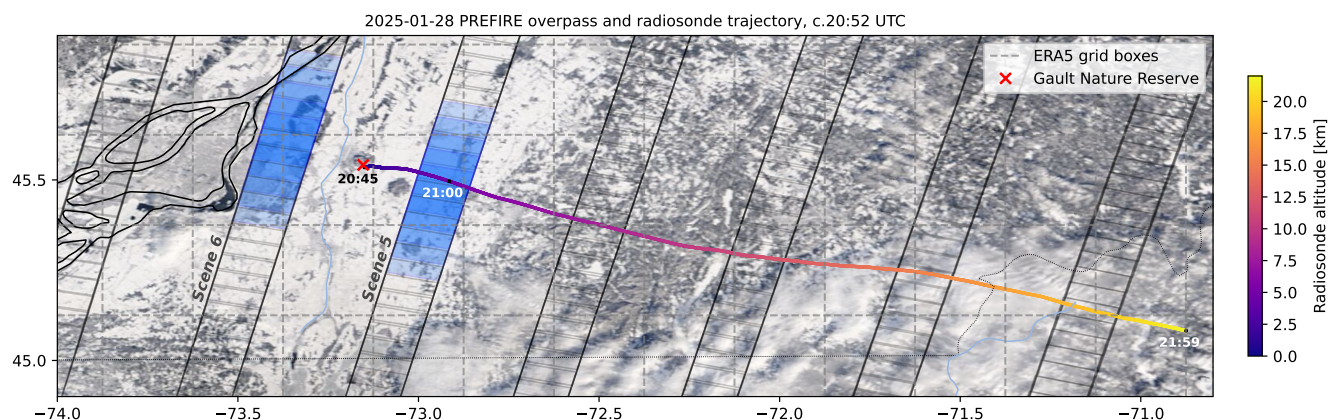


**Figure 2.** Map showing the layout of measurements for our case study. The red cross marks the the Gault Nature Reserve site, where FINESSE was located. The track of the radiosonde launched from here is shown, with times (UTC) labelled throughout the flight and colours indicating its altitude. Solid boxes across the image indicate the PREFIRE FOV polygons from the overpass, with significant overlap in the along-track direction (approx. north-east–south-west). FOVs selected for averaging in the scenes 5 and 6 are shaded blue. Grey dashed lines indicate the ERA5 grid boxes for reference. The background image is from MODIS Terra observations, approx 6 hours before the PREFIRE overpass (Credit: NASA).

The spectral emissivity and radiating temperature of the surface are needed in addition to simulate infrared radiation upwelling  
 135 to space.

For this study, we make use of a range of atmospheric data sources. Firstly we use ERA5 hourly profiles of temperature, specific humidity, and ozone concentration as a function of pressure on 137 atmospheric model levels, at a horizontal resolution of 0.25° (Hersbach et al., 2020). We also use the corresponding ERA5 estimates of the surface skin temperature ( $T_{sfc}$ ).

Secondly, radiosondes launched periodically during the WHAFFERS campaign also measured profiles of temperature and  
 140 humidity. The radiosonde model used during WHAFFERS was the InterMet Systems iMet-4 radiosonde. In the literature, we found limited prior studies using this model (see e.g. Ghysels et al., 2024; Liu et al., 2024) or brand (Hurst et al., 2011; Flores et al., 2013); its performance has not been independently and systematically reviewed. Figure 2 shows the track of the radiosonde launched at 20:45 UTC on 28th January 2025, with the PREFIRE observation footprints from the c.20:52 UTC overpass overlaid. Temperature, relative humidity, altitude, and pressure measured by the radiosonde are available at 5 m  
 145 vertical intervals.

Finally, during the WHAFFERS campaign, near-surface meteorological data were recorded continuously at the Gault Nature Reserve at a weather station within 50 m of FINESSE. Measurements of relevance to our study are from eight Vaisala HMP155A probes at different heights up to 10 m above ground, with temperature and relative humidity readings taken every minute. Analysis of these data over several measurement days indicated that probes at 1.5 m and 3.5 m above ground level were  
 150 consistently biased and so their readings have been discarded.



The emissivity of the surface ( $\varepsilon_{\text{sfc}}$ ) is taken from the dataset compiled by Huang et al. (2016) which provides modelled estimates of spectral emissivity at nadir-view for a variety of surface types and is the only dataset to offer this into the far-infrared. The ‘medium snow’ surface type (with median grain size 600  $\mu\text{m}$ ) is used in this study; fine and coarse snow as well as ice surface types are also available.

155 Concentrations of  $\text{CO}_2$ ,  $\text{CH}_4$ , and  $\text{CO}$  are taken from the CAMS global greenhouse gas forecasts (Agustí-Panareda et al., 2019). For  $\text{N}_2\text{O}$  and  $\text{SF}_6$ , we take mixing ratios from NOAA’s Global Monitoring Laboratory (NOAA), while for CFC-11, CFC-12 and  $\text{CCl}_4$  concentrations are estimated by extrapolating the average 5-year trend of Atmospheric Histories (Bullister and Warner, 2017). Mixing ratios of the latter five greenhouse gases are assumed constant with height.

The different sources of atmospheric data are combined to generate profiles specifically for downwelling (FINESSE) and  
160 upwelling (PREFIRE) radiance simulations. To probe the impact of the characterisation of the atmosphere on the associated radiances, in each case we create two sets of temperature and humidity profiles. The ‘ERA5’ set is based purely on the closest ERA5 profile in space and time (45.5° N, 73.25° W, 21:00 UTC), while the ‘in-situ’ set is based primarily on the available in situ measurements. Table 1 provides a summary of the inputs to each set and the associated nomenclature we use to refer to each simulation. Apart from atmospheric temperature and humidity, all components described above are specified identically  
165 for the ERA5 and in-situ simulations. The same surface and atmosphere is used to simulate both TIRS scenes 5 and 6.

The only difference between the ERA5-DW and ERA5-UW profile is the choice of the lower boundary. For the former, we take the observation level as 130 m above sea level, consistent with FINESSE’s altitude on a hillside at the Gault site. For the latter we use the entire ERA5 vertical profile (which has a surface altitude of 30 m). There are more substantial differences between the in-situ-DW and in-situ-UW cases. For the former we replace the radiosonde profile between 130–140 m with  
170 values from the weather station tower. For the latter, we do not use the weather station measurements and instead supplement the radiosonde values with co-located ERA5 data between 130 m and the surface. Similarly, in both cases, at altitudes above the maximum extent of radiosonde measurements we add the ERA5 data. The radiosonde data used in the in-situ profiles is smoothed from its native 5 m resolution before simulation.

Temperature and water vapour mixing ratio profiles for the ERA5 and in-situ cases are shown in Fig. 3. The insets highlight  
175 the near-surface conditions crucial for simulating FINESSE measurements. The profiles of temperature are broadly similar, with some differences reaching up to 5 K in parts of the free troposphere. The near-surface temperatures measured by the radiosonde immediately after launch are around 0.5–1 K warmer than the corresponding ERA5 values, behaviour which is not seen in the weather station observations. This does lead to a distinct feature in the in-situ-UW profile where the ERA5 and radiosonde profiles are joined, but sensitivity studies confirmed this has negligible impact on simulated upwelling radiances at  
180 the top of the atmosphere. The two water vapour profiles are more different; while both show a moist layer of similar extent at c.500 hPa, water vapour varies significantly below that. Overall, the in-situ profiles indicate a drier atmosphere.

## 2.4 Radiative transfer modelling

Simulated radiances at the top of atmosphere and at the surface are generated using the Line-by-Line Radiative Transfer Model (LBLRTM, Clough et al., 2005). Its high accuracy has led to it becoming a standard benchmark for spectrally resolved radiative



**Table 1.** Data sources used to specify temperature and water vapour concentration across altitude regimes (left-hand column) for the different atmospheric profiles simulated. Simulated surface properties are also shown for PREFIRE observations. The marking “—” indicates that no simulation of this level was performed in this case. Specification of other gases is identical across the four profiles and is detailed in the text.

Instrument	FINESSE		PREFIRE	
Profile shorthand	ERA5-DW	In-situ-DW	ERA5-UW	In-situ-UW
>21.8 km		ERA5		ERA5
140 m–21.8 km	ERA5	Radiosonde (smoothed)	ERA5	Radiosonde (smoothed)
130–140 m		Weather station		
<130 m	—	—		ERA5
Surface	—	—	$T_{sfc}$ : ERA5; $\varepsilon_{sfc}$ : Huang et al. (2016)	

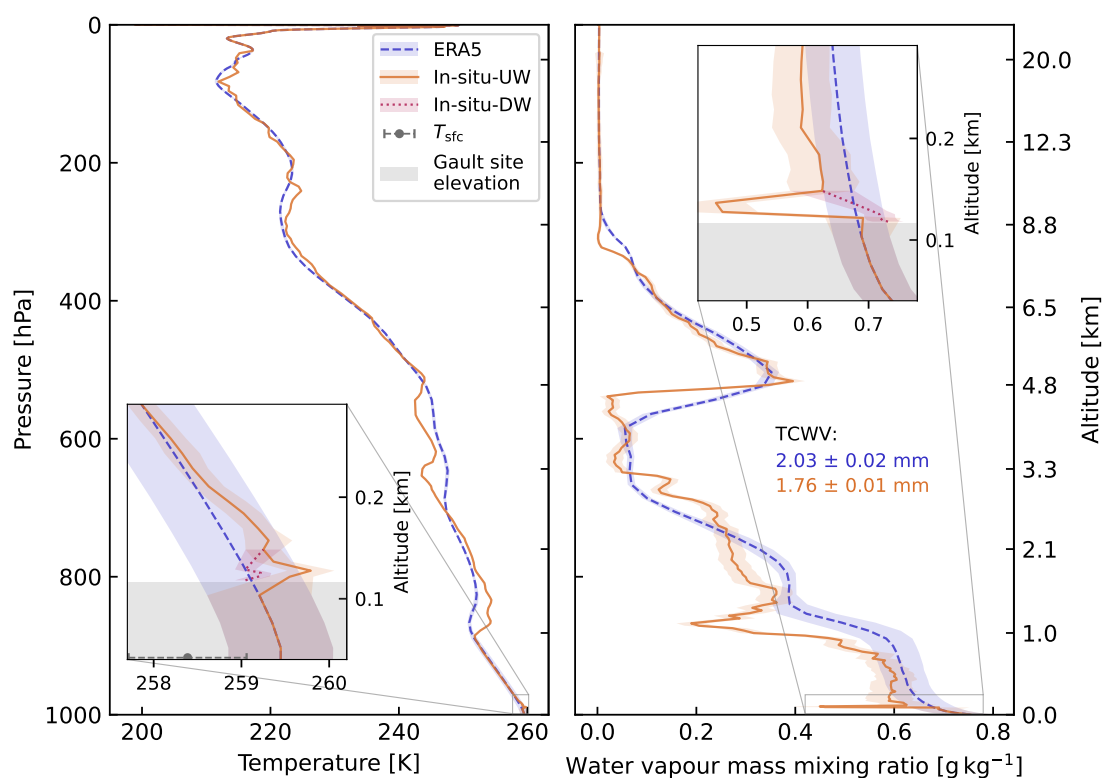


**Figure 3.** Profiles of temperature (left) and water vapour (right) for the cases simulated, with coloured shading showing the respective uncertainties. The ERA5-DW and -UW profiles use the same data. The dotted line indicates where the in-situ-DW profile differs from the in-situ-UW profile; above this, the two in-situ profile specifications are identical. Grey shading in the inset plots indicates the elevation of the Gault site; data below this is neglected for downwelling (DW) simulations. The skin temperature from ERA5, used in both upwelling simulations, is shown in the temperature inset plot. Colour-coded text shows the total column water vapour (TCWV) for ERA5-UW and in-situ-UW profiles (right).



185 closure experiments (e.g. Delamere et al., 2010; Sussmann et al., 2016; Mlawer et al., 2019) and for evaluation of other radiative transfer codes (e.g. Oreopoulos et al., 2012; Hogan and Matricardi, 2020). For this work, we use LBLRTM v12.17, including spectral lines from AER Line File v3.8.1, and the MT\_CKD v4.3 water vapour continuum model (Mlawer et al., 2023).

We input the profiles described in Sect. 2.3 to LBLRTM, simulating the effects of the first 30 molecules listed in the HITRAN database. For those gases not mentioned above, we use the LBLRTM ‘mid-latitude winter’ default values.

190 To simulate the PREFIRE and FINESSE measurements, instrument characteristics must be applied to the very high resolution radiances calculated by LBLRTM. For PREFIRE, the radiance from each channel of the grating spectrometer is calculated by integrating the LBLRTM output with the normalised channel spectral response function (v13, PREFIRE team, 2025). To simulate FINESSE radiances, spectra are converted to interferograms and truncated to mimic the effects of an ideal Fourier-transform spectrometer with FINESSE’s maximum optical path difference. After converting the truncated interferograms back to spectra, they are convolved with a spectrally dependent instrument line shape as described by Murray et al. (2024), which  
195 simulates asymmetries in FINESSE’s optical path.

### 3 Uncertainties and challenges in closure analysis

#### 3.1 Spatial collocation

In the discussion of the experimental setup thus far we have assumed that all data sources and instruments describe or measure  
200 the same atmospheric column. Since this is not the case, we examine here the effect of imperfect horizontal collocation in our measurements.

We use ERA5 fields to estimate the spatial variability in the scene meteorology at scales larger than the ERA5 horizontal scale of  $0.25^\circ$ . In the absence of horizontal wind, the radiosonde would sample only the atmospheric column immediately above FINESSE. In reality, the wind advects the radiosonde some 185 km east of the Gault reserve over its flight. We construct  
205 a profile which ‘follows’ the radiosonde trajectory and samples from the spatially and temporally closest ERA5 grid cells (termed ‘ERA-following-sonde’ as shorthand), assuming that the ERA5 fields are representative of the true spatial variability of the scene meteorology. The radiances from this profile are simulated as described in section 2 and compared to those using the standard ERA5 profile; this comparison is shown in Fig. 4a and b. This offset is included as an uncertainty for the in-situ simulations.

210 As demonstrated in Fig. 2, the PREFIRE FOVs 5 and 6 lie either side of the Gault site, and so do not pass directly over FINESSE. To assess the impact this has, we simulate the radiances from the ERA5 grid points contained in the PREFIRE footprints. The comparison between these and radiances simulated from the closest grid point to the Gault site is shown in Fig. 4. The average of these offsets, weighted by the number of FOV midpoints falling in each box, is included as an uncertainty source for the PREFIRE simulations.

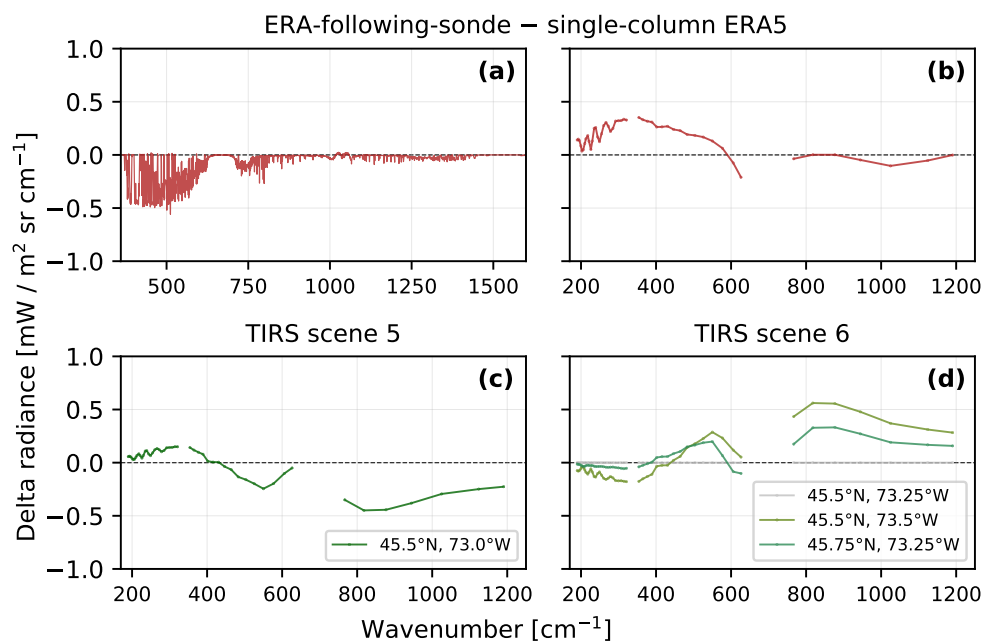


**Figure 4.** Top row: differences in simulated FINESSE (a) and PREFIRE (b) radiances when using a profile of ERA5 data ‘following’ the radiosonde track, compared to a single ERA5 column at the Gault site. Bottom row: differences in simulated PREFIRE radiances for TIRS scene 5 (c) and 6 (d) simulated using various ERA5 grid points located within the instrument FOV, compared to that closest to the Gault site (45.5° N, 73.25° W).

### 215 3.2 Instrument performance

Uncertainties in FINESSE radiances are well-characterised and fully described by Murray et al. (2024). Briefly, the noise-equivalent spectral radiance (NESR) is a random error resulting from spectrally uncorrelated detector noise and can be reduced through averaging, while other uncertainties arise from the calibration process. For the measurement conditions of our study, these are both shown in Fig. 5a.

220 Uncertainties in the PREFIRE radiances are quantified as noise-equivalent radiances, shown in Fig. 5b. Some elements of the detector array are known to have high noise or responsivity faults and we have masked their readings. This leads to some gaps in the FIR spectra. Channels in the FIR-2 band are flagged as having ‘uncategorised calibration’ due to uncharacterised instrument issues. Uncertainty in PREFIRE calibration (i.e. absolute radiometric accuracy) is not known. Information on PREFIRE observational issues identified prior to launch is detailed by Drouin et al. (2025), and post-launch in section 4 of the  
 225 PREFIRE radiance product R01 user guide (Hokanson Wagner et al., 2025).

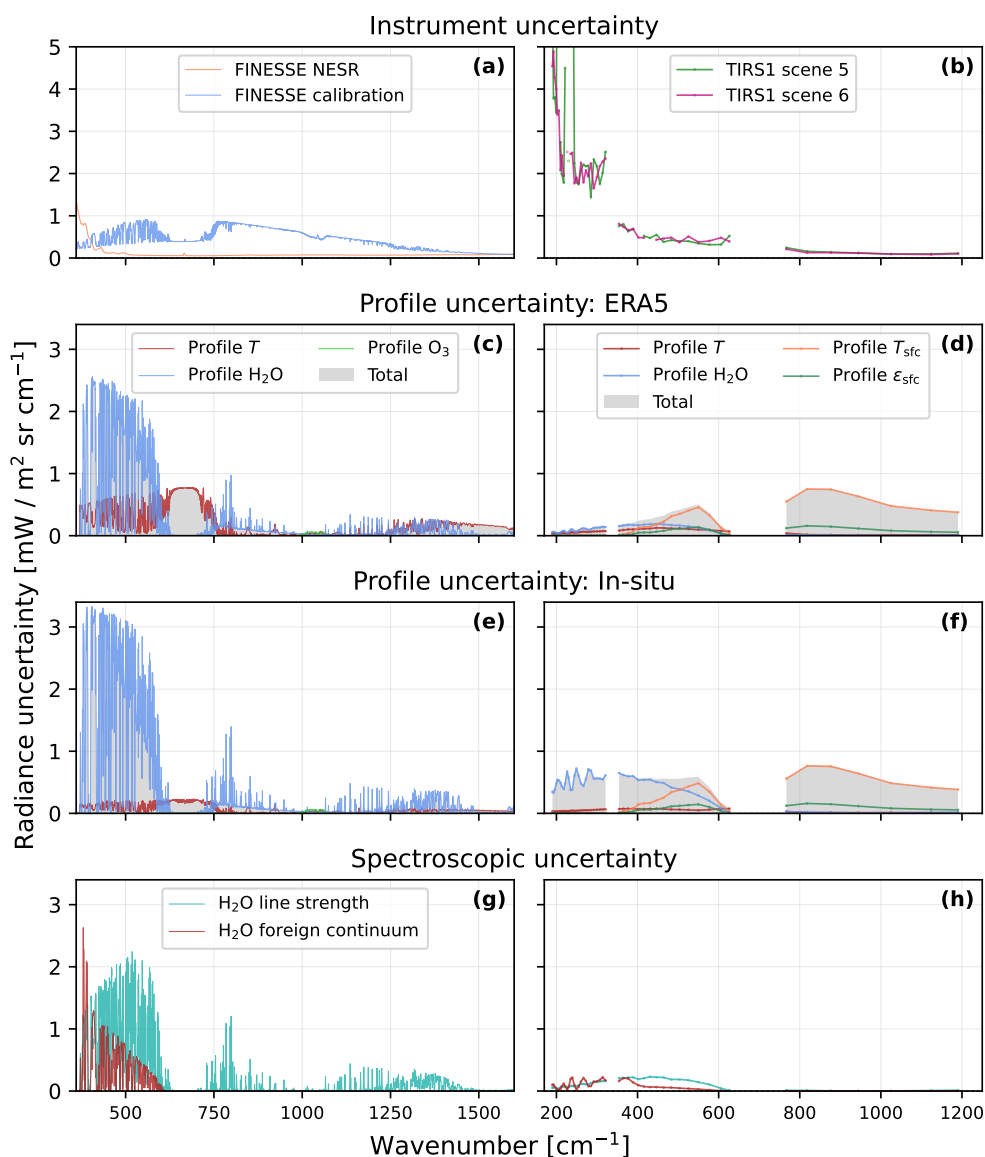


**Figure 5.** Estimates for several sources of uncertainty considered in the closure experiment. The left column (**a**, **c**, **e**, **g**) is for FINESSE, the right (**b**, **d**, **f**, **h**) for PREFIRE. (**a**, **b**): uncertainty in measured radiances due to instrument noise and calibration. (**c**–**f**): uncertainty in simulated radiances due to uncertainty in the various labelled profile quantities; the legends in (**c**) and (**d**) apply also for (**e**) and (**f**) respectively. (**g**, **h**): uncertainty in simulated radiances following from uncertain H<sub>2</sub>O spectroscopic parameters; the legend in (**g**) applies to both plots. Note the different *y*-scale used in (**a**, **b**) compared to other rows.



### 3.3 Constraining atmospheric and surface states

Quantification of the uncertainty in the input atmosphere and surface profiles varies by data source. For ERA5 data, we represent the uncertainty in reanalysis quantities using the standard deviation of the accompanying 10-member ensemble. Uncertainties in readings from the radiosonde and weather station are calculated using information from the respective manufacturers' data sheets (InterMet Systems, 2022; Vaisala, 2025). 'Calibration uncertainty' or 'repeatability in calibration' figures are treated as systematic uncertainties and 'accuracy' or 'combined uncertainty' figures as random uncertainties. Surface emissivity uncertainty is estimated as the spectrally averaged spread in the fine, medium, and coarse snow types in the dataset. These uncertainties encompass temperature, humidity, ozone concentration, surface temperature, and surface emissivity; uncertainty in other quantities supplied to the radiative transfer code is considered negligible. Uncertainty estimates for temperature, water vapour mixing ratio, and  $T_{\text{sfc}}$  are shown in Fig. 3.

For a simulated total state vector  $\mathbf{x}$ , the uncertainties described above may be represented as a pair of vectors  $(\boldsymbol{\sigma}, \mathbf{s})$  of random and systematic errors respectively. These vectors have components  $(\sigma_i, s_i)$  for the level  $i$  where  $s_i$  may be zero if there is no systematic uncertainty considered. We tackle random and systematic uncertainties separately to calculate a sample set of realistic errors in the total state vector, represented  $\delta_m \mathbf{x}$  (the  $m$  subscript labelling the samples). For random errors, we construct a covariance matrix such that they are correlated between nearby atmospheric levels. This matrix  $\mathbf{C}$  has terms defined by

$$C_{ij} = \sigma_i \sigma_j \exp\left(-\frac{|z_i - z_j|}{h}\right), \quad (1)$$

with  $z_i$  the altitude of level  $i$  and  $h$  some vertical scale height (Rodgers, 2000; Feldman et al., 2008). Sample random profile errors  $\delta_m \mathbf{x}_{\text{rand}}$  are randomly sampled from a multivariate normal distribution with mean  $\boldsymbol{\sigma}$  and covariance  $\mathbf{C}$ . Conversely, systematic errors are modelled as fully vertically correlated. In practice, this means that sample systematic profile errors  $\delta_m \mathbf{x}_{\text{sys}} = z_m \times \mathbf{s}$ , with  $z_m$  sampled from a standard normal distribution. These random and systematic sources are then added for each sample:  $\delta_m \mathbf{x} = \delta_m \mathbf{x}_{\text{sys}} + \delta_m \mathbf{x}_{\text{rand}}$ .

Using LBLRTM, the Jacobian  $\mathbf{J}$  is then evaluated as  $J_{ij} = \frac{\partial y_i}{\partial x_j}$  for a spectral point  $i$  and some state variable  $x_j$  at layer  $j$ . The instrument response is applied to the output high-resolution Jacobians as described in Sect. 2.2. Sample profile uncertainties  $\delta_m \mathbf{x}$  are propagated to sample spectral uncertainties  $\delta_m \mathbf{y}$  using  $\delta_m \mathbf{y} = \mathbf{J} \delta_m \mathbf{x}$ . The overall spectral uncertainty  $\delta \mathbf{y}$  is calculated as the standard deviation of the  $\delta_m \mathbf{y}$ , using 5000 samples. This is repeated for each variable considered. For FINESSE these variables are temperature, and water vapour and ozone concentrations. We found that PREFIRE had little sensitivity to ozone concentration uncertainty, so we consider temperature, water vapour concentration, surface temperature and emissivity.

The in-situ profiles have a significant error contribution from systematic uncertainties which dominates over random uncertainties; as such these profiles have little sensitivity to the choice of  $h$ . We found some sensitivity to the choice of  $h$  for the ERA5 profile uncertainty, having only random errors. For a similar quantity to  $h$  in the literature, Rodgers (2000, Ch 2) use the atmospheric scale height and Ridolfi et al. (2022) use a 5 km correlation in retrieval covariances, Warwick et al. (2022) find a vertical correlation length of 0.8 km for temperature and water vapour in the Met Office UM, and from measurements Fischer et al. (2013) suggest a non-convective water vapour correlation of 0.23 km. Investigating across this range, we found



260 that radiance uncertainties due to water vapour errors varied by a factor of 3; we choose a value of  $h = 1.5$  km for temperature and water vapour in this work, representing a slightly conservative middle ground. The resulting uncertainties in simulated radiances are shown in Fig. 5c–f.

### 3.4 Water vapour spectroscopy

265 Since we use a relatively fine vertical resolution and perform line-by-line calculations, the most significant uncertainties in the radiative transfer forward modelling come from either the input spectroscopic data or in the assumptions used to model spectroscopic phenomena such as spectral line mixing. We neglect investigation of line mixing uncertainty and instead focus on the uncertainty from water vapour spectroscopy as the dominant and most variable absorber in this case. In particular, we consider uncertainties in H<sub>2</sub>O line strengths and in the absorption coefficients of the FIR components of the H<sub>2</sub>O foreign continuum, similar to Mosselmans et al. (2026). We found that uncertainties in the line positions had a negligible effect on the simulated spectra. We also neglect any uncertainties in absorption coefficients for other parts of the water vapour continuum, as (a) foreign continuum absorption is substantially smaller at larger wavenumbers, and (b) the self-continuum absorption will be small anyway in this case due to the very dry atmosphere.

270 Water vapour line strengths are perturbed according to the assigned uncertainty code in the AER Line File, while foreign-continuum absorption coefficients are perturbed by the uncertainty values assigned by Mlawer et al. (2019). LBLRTM is then re-run using this perturbed spectroscopy. The resulting difference of this compared to a simulation with unperturbed spectroscopy is taken as the spectral uncertainty due to spectroscopic uncertainties. These uncertainties are presented in Fig. 5g and h.

In our results, we combine the spatial collocation, instrument, forward-modelled profile, and spectroscopic uncertainties in quadrature to form a total uncertainty for each of the four simulations.

## 280 4 Results

To assess radiative closure, we subtract the spectra measured by the FINESSE and PREFIRE TIRS instruments from the spectra simulated as described in sections 2.3 and 2.4. This difference is termed a ‘residual’, representing the offset of measurements from simulations. These residuals are compared to the bounds given by the total uncertainties calculated in Sect. 3.

285 We begin by discussing residuals for the FINESSE instrument, shown in Fig. 6. In these cases, a positive residual indicates more emission by the overlying atmosphere in the simulation than was recorded in reality. For the viewing geometry here, this typically means either too much gas and/or too warm an atmospheric temperature; the inverse is true for negative residuals.

In both FINESSE cases, the residuals are generally close to zero throughout and mostly within the bounds of the uncertainty, indicating good agreement between observations and simulations. A large negative spike around  $597.6\text{ cm}^{-1}$  is attributed to deficiencies in the LBLRTM line coupling modelling used for CO<sub>2</sub> and has been noted in other studies (e.g. Delamere et al., 2010; Mosselmans et al., 2026). We expect that the negative spike at  $392\text{ cm}^{-1}$  is related to the higher instrument noise at the edge of the FINESSE detection capability. A large positive spike at  $667\text{ cm}^{-1}$  is caused by the absorption and emission of the

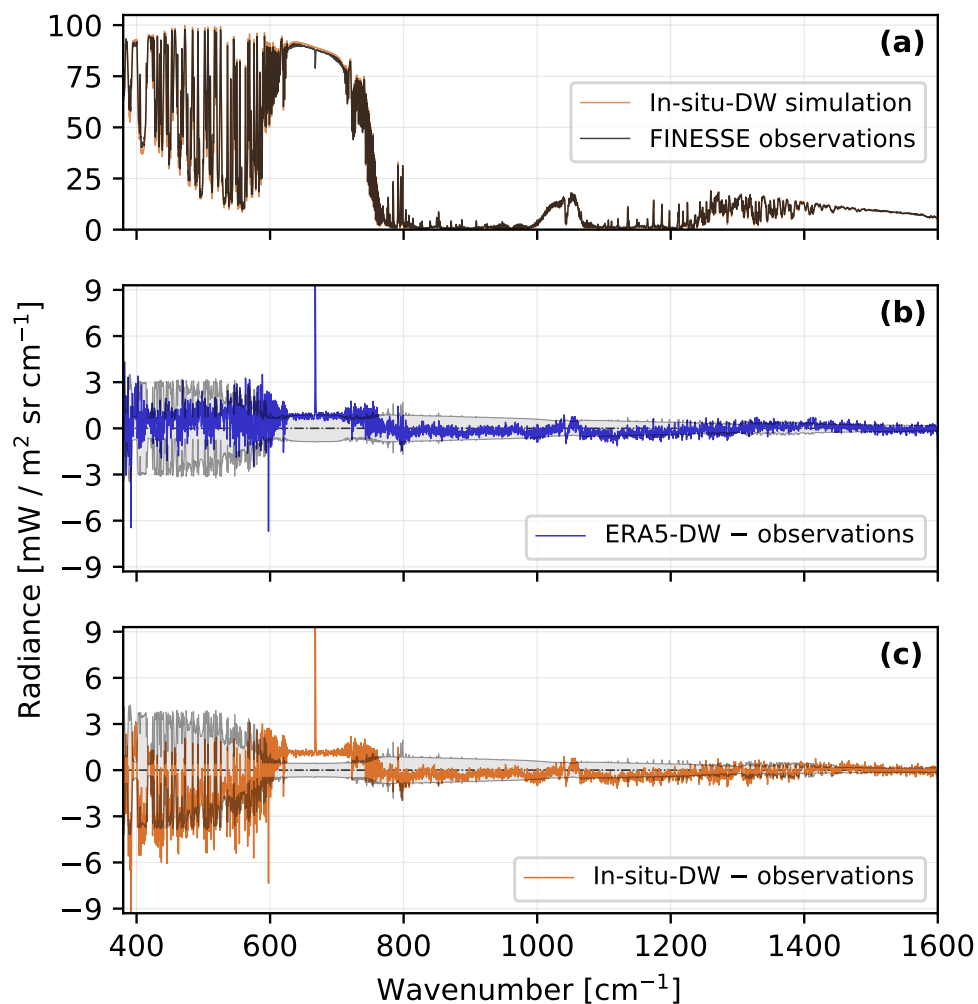


**Figure 6.** (a) FINESSE observations (black) and the in-situ-DW simulation for comparison. (b): residuals for the ERA5-DW simulation compared to observations. The grey shading and line indicate the total uncertainty limits described in Sect. 3. (c): as in (b), but for the in-situ-DW simulation.



CO<sub>2</sub> molecule; at this frequency it is so strong that only the cold air inside the instrument is sensed. Nearby wavenumbers are also quite opaque, so the positive bias of this feature in both ERA5 and in-situ profiles indicates that near-surface atmospheric temperatures are too warm in the simulated profiles.

295 In the mid-infrared (for FINESSE, 667–1600 cm<sup>-1</sup>) outside of the influence of CO<sub>2</sub>, the FINESSE residuals in both cases are very small and close to zero, without notable excursions from the uncertainty bounds. There is little downwelling radiance in the region, but the small residuals point towards a reasonably good specification of methane (1200–1400 cm<sup>-1</sup>) and water vapour (1300–1600 cm<sup>-1</sup>). Within the infrared window, agreement around the ozone absorption band (1000–1100 cm<sup>-1</sup>) implies an accurate specification of ozone concentrations and upper-atmospheric temperatures. A very small negative bias within the  
300 uncertainty bounds is noted throughout the atmospheric window; this could be caused by emission from aerosols or trace species which are not simulated.

In the far-infrared, the ERA5-DW residuals are almost entirely within the uncertainty bounds. The slight positive bias in this region strongly affected by water vapour would suggest the simulated profile having slightly too warm or moist conditions, especially near the surface. Having too high a simulated near-surface temperature would be consistent with the positive residual  
305 in the (620–720 cm<sup>-1</sup>) CO<sub>2</sub> spectral feature. We note an unexplained deviation beyond the uncertainty limits around 395 cm<sup>-1</sup> but this is likely due to instrument noise, again being on the edge of the detection range.

The in-situ-DW residuals in the FIR have a negative bias, with the residual for many wavenumbers lying below the lower uncertainty bound for this case. We conclude from the spectral range of this bias, the profile in Fig. 3, and the near-surface warm bias of the simulated atmosphere diagnosed from the CO<sub>2</sub> emission feature, that this FIR negative bias is caused by the  
310 radiosonde recording less total water vapour than is present in the atmosphere.

The PREFIRE residuals in Fig. 7 are separated by cross-track TIRS scene to account for the different sensor characteristics, viewing angle, and FOV geographies. Here, a positive residual may indicate the simulation has too warm or emissive a surface or atmospheric layer, or too transparent an atmosphere (transmitting more radiation from warmer levels below and from the surface than in reality). In spectral regions common to both instruments, the PREFIRE residuals generally have a slightly larger  
315 magnitude, and much greater spectral variation, compared to FINESSE residuals degraded to PREFIRE spectral resolution (not shown). The effect of the large instrument noise in the FIR-2 band (185–330 cm<sup>-1</sup>) is clear, with significant scatter even after averaging over five spectra.

The features of the residuals in the MIR-2 band show little difference between the ERA5-UW and in-situ-UW simulations; this is to be expected, as the simulations have identical specification of surface temperature, surface emissivity, and ozone  
320 concentrations. These are the main factors controlling radiances in this region under these conditions. The MIR-2 residuals exhibit a similar pattern in both cross-track scenes, with a slight spectral zig-zagging. In all comparisons residuals are positive in this region indicating too much modelled radiation from the surface, indicating either too warm or too emissive a surface in the simulations.

Turning to the far-infrared bands, the difference between the ERA5-UW and in-situ-UW simulations becomes somewhat  
325 clearer. For both scenes in the dirty window (FIR-1 band), the ERA5-UW residuals lie slightly closer to zero than those for in-situ-UW. This matches the findings of too dry an atmosphere from the radiosonde readings; the in-situ-UW simulated

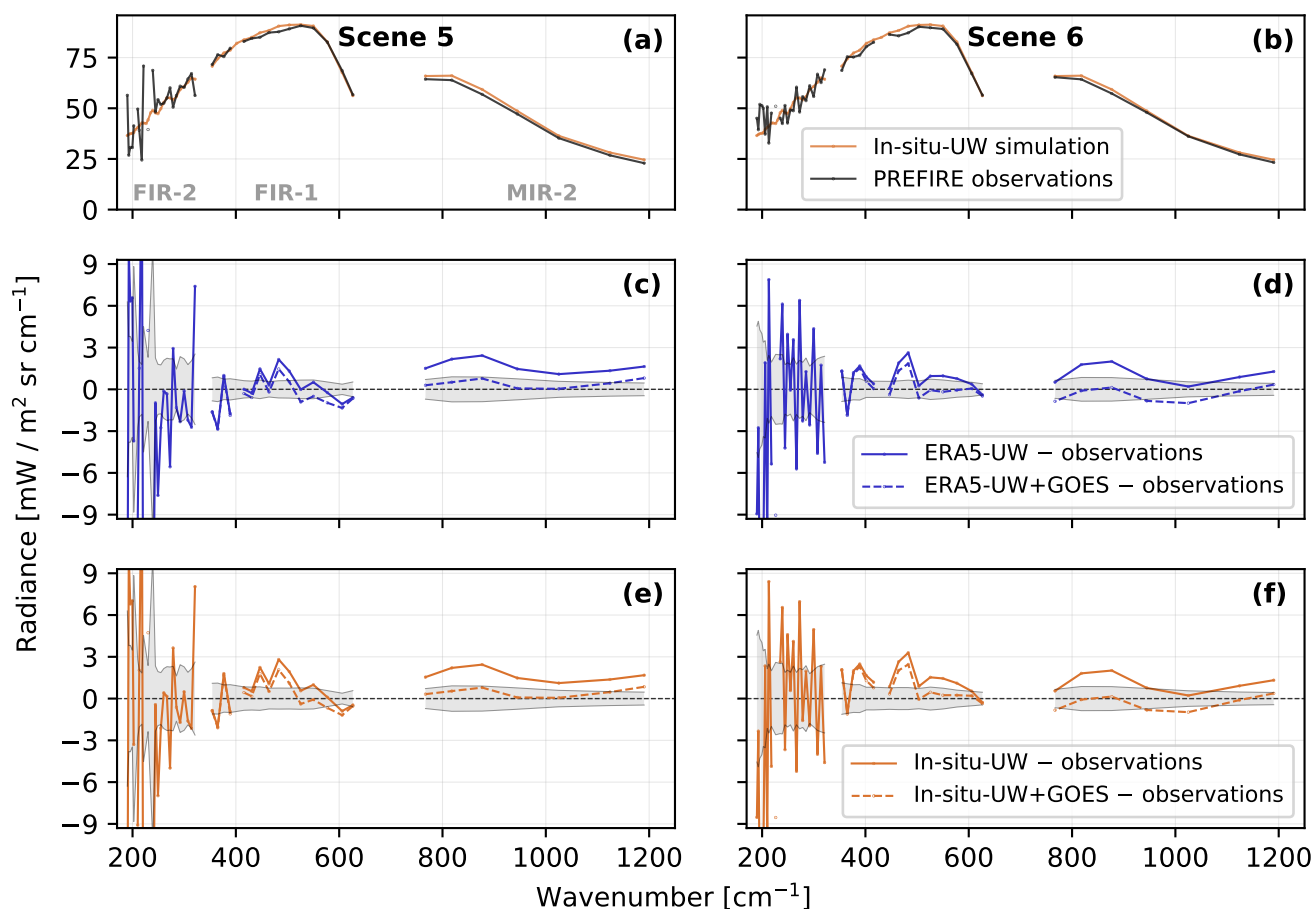


**Figure 7.** (a, b) PREFIRE observations (black) and the in-situ-UW simulation for comparison. (c, d): residuals for the ERA5-UW simulation compared to observations. Additional dashed lines indicate residuals for a simulation using land surface temperature observations from the ABI on GOES-16. The grey shading and line indicate the uncertainty limits described in Sect. 3. (e, f): as (c, d), but for the in-situ-UW simulation. The left column (a, c, e) shows the TIRS scene 5 radiances, and (b, d, f) shows TIRS scene 6. The grey text in (a) labels the spectral bands of the TIRS instrument.



atmosphere is more transparent in this spectral range and so permits more thermal radiation to escape to space from the (near-)surface than is observed. A slight positive bias in the residuals in scene 6 could also point to issues with the surface specification. In the FIR-2 band ( $170\text{--}340\text{ cm}^{-1}$ ), the number of points lying outside of the uncertainty bounds suggests that the total radiance uncertainty of the instrument is underestimated at present; the instrument noise makes further quantitative deductions difficult.

#### 4.1 Use of GOES ABI surface temperature

The findings of a consistent positive bias of simulations relative to PREFIRE observations in the infrared window region prompts a re-evaluation of the simulated surface properties. Surface emissivities in the mid-infrared are sufficiently well-constrained and constant across surface types to preclude this being the sole cause of the residuals seen, so we explore modifications of the emitting skin temperature.

To find an alternative source of this  $T_{\text{sfc}}$ , we turn to observations from geostationary platforms. Specifically, from the GOES-16 satellite we take the Advanced Baseline Imager's (ABI) full-disk land surface temperature retrieval (ABI-L2-LST). This is sampled at 21:00 UTC, just seven minutes after the PREFIRE overpass, and has a 10 km resolution at nadir. For each PREFIRE scene, we take an average of the ABI retrieved land surface temperature readings within the TIRS FOV polygons weighted by area and overlap fraction. The resulting temperatures ( $256.8 \pm 0.7\text{ K}$  and  $256.7 \pm 0.6\text{ K}$  for scenes 5 and 6 respectively) then replace the ERA5  $T_{\text{sfc}}$  in otherwise identical simulations.

The resulting residuals from the simulations with modified  $T_{\text{sfc}}$  are shown as dashed lines in Fig. 7. In the MIR-2 band, the inclusion of the ABI  $T_{\text{sfc}}$  significantly improves the residuals, with most channels' residuals now lying within the uncertainty bands. In the FIR-1 band an improvement is clear for both simulations in scene 6, while any improvement in scene 5 is marginal.

## 5 Discussion

Given the excellent agreement of the ERA5-DW simulation with observations by the FINESSE instrument, we infer that this profile represents a robust knowledge of the overlying atmosphere. The corresponding simulation for PREFIRE, when using the observed ABI  $T_{\text{sfc}}$ , also lies close to the observations, but slightly more spectral points lie outside the uncertainty limits than would be expected, especially in the FIR-2 band. We believe that these anomalous residuals are mostly a result of instrument effects. In the MIR-2 and FIR-1 bands, where residuals show a similar pattern for the two scenes, the similarity hints at a common cause warranting further investigation, such as calibration error remaining even after the radiance bias correction. In the FIR-2 band, the cause is likely detector noise, which is perhaps underestimated at present. We note that the current PREFIRE L1B products mark all FIR-2 band channels with a flag indicating the quality is unknown and that there may be calibration biases. It is worth highlighting that for both FINESSE and PREFIRE, the largest uncertainties are found in the far-infrared.

The detailed analysis of uncertainties in Sect. 3 allows us to identify the main sources of uncertainty in the experiment. For FINESSE, specification of water vapour profiles is a large source of uncertainty in both simulations, especially in the FIR.



This is slightly larger in the in-situ case, where we have treated systematic errors in the radiosonde measurements as fully  
360 vertically correlated. The residuals shown in the in-situ-DW case, however, lead us to question the veracity of the radiosonde  
measurements. Several studies have noted dry biases in radiosonde measurements, particularly in dry conditions (Vömel et al.,  
2007; Rowe et al., 2008; Miloshevich et al., 2009; Dzambo et al., 2016). Our results suggest a similar dry bias for the iMet-4  
radiosonde as used in the WHAFFERS campaign, which has not yet been thoroughly investigated.

Given the radiosonde residual bias in the FIR and the good performance of the ERA5-DW profile, we investigate a bias  
365 correction method. The total moisture content of the column measured by radiosondes over the entire WHAFFERS campaign  
was calculated and compared to values calculated from ERA5 following each radiosonde track (as in Sect. 3.1). Of the ten  
launches without issue, seven featured very low column water vapour  $< 3$  mm. Across these seven cases, the radiosonde  
measurements exhibit a consistent dry bias of about 9 % relative to ERA5 (i.e.  $CWV_{\text{sonde}} \approx 0.91 \times CWV_{\text{ERA5}}$ ). Remedying  
this bias by a scalar adjustment of the radiosonde-measured water column and re-running the experiment much improves  
370 agreement with the bias-adjusted in-situ-DW case, even outperforming the ERA5-DW case in the FIR (not shown). We thus  
conclude that it is likely that the radiosonde has dry humidity bias in these conditions. However, we also cannot rule out the  
possibility that this radiosonde bias is caused by campaign-specific errors in the launch process.

We recommend that for closure experiments, radiosondes be used in tandem with either a trusted bias correction algorithm  
or an auxiliary source of information. This information could come from reanalysis, as in our brief investigation, but ideally  
375 it would be from collocated measurements, such as retrievals from microwave sensors. We argue further that passive remote  
sensing in spectral regions different to those measured by the closure-targeting instrument is crucial to ensure independence of  
observations from simulations. Uncertainties in the FIR spectroscopy of water vapour also have a sizeable impact on modelling  
FINESSE radiances. Further closure or laboratory studies may be able to address this.

The appearance of some residuals beyond uncertainty for FINESSE between  $390\text{--}400\text{ cm}^{-1}$  in both simulations was inves-  
380 tigated by comparing the simulated and measured radiances to 160 spectra acquired over a 60 minute window, each one an  
average of 20 scans. The many individual spectra showed a large spread in which the residual signal was not an outlier (not  
shown). The fact that residuals lie beyond the uncertainty limits could indicate that the FINESSE NESR is under-reported in  
this region, and/or that the extension of FINESSE to  $380\text{ cm}^{-1}$  requires further validation.

Finally for FINESSE, characterising the air temperature very near the instrument is key. There are some significant residuals  
385 for wavenumbers with strong sensitivity to the surface layers, especially in the  $\text{CO}_2$  emission features (c.  $600\text{--}750\text{ cm}^{-1}$ ).  
Readings from FINESSE's auxiliary temperature sensor were anomalous in this field campaign and so not used; ensuring valid  
measurements from this sensor could enhance the robustness of future closure tests with FINESSE.

PREFIRE closure diagnosis in the FIR, particularly in the FIR-2 band, is largely hindered by instrument noise. Further  
evaluation of persistent biases could be possible using substantial averaging. In similar conditions to this study, this noise  
390 would no longer be a dominant uncertainty source in the FIR-1 band after averaging over 10 spectra, or 150 spectra in the FIR-  
2 band, for PREFIRE satellite 1. Satellite 2 has a higher instrument noise which would require approximately twice as many  
spectra. A study using a set-up like ours employing an averaging approach would hence require a long-term ground-based  
spectrometer data record (possibly over 12 months to build up the clear sky statistics required, though latitude dependent),



and may not be able to use radiosonde data for the quantity of overflights needed. Uncertainty in the radiosonde water vapour  
395 specification is comparable to instrument noise around  $350\text{--}500\text{ cm}^{-1}$  and would become a leading uncertainty source with  
more averaging of spectra, reinforcing the need for precise water vapour measurements in FIR closure studies.

In the MIR, the dominant uncertainty for PREFIRE is due to the temperature of the underlying surface, with its emissivity  
also playing an important role. The importance of the surface temperature in this setup is further reinforced by the finding of  
a drastic improvement, in this instance, of taking this figure from the GOES ABI rather than ERA5. Due to the large area of  
400 the measured swath, a ground-based temperature or emissivity measurement would likely only be representative for a very  
homogeneous surface. Another possibility is to remotely sense the surface temperature with a drone-mounted instrument in  
the region around the ground station; this platform could then additionally sample the nearby variation in the humidity field.  
Radiances observed by a low-flying aircraft could also be used to retrieve surface temperature and emissivity separately, as  
demonstrated by Bellisario et al. (2017).

405 There is also further opportunity for satellite-to-satellite validation of PREFIRE, in the MIR spectral region, using geosta-  
tionary satellites. They offer coverage over a large swath with much shorter repeat times than polar-orbiting missions. The  
Infrared Sounder on the Meteosat Third Generation (MTG-IRS) will provide spectrally resolved mid-infrared radiances from  
a geostationary platform. This could yield plentiful opportunities to perform radiance comparisons under a range of conditions  
for the PREFIRE MIR channels. Here a key issue to resolve would be the impact of viewing geometry.

410 Finally, we note that the simulations performed for this study have already proven useful in validating improvements in the  
second release of the PREFIRE L1B radiance product (though direct comparison of simulations to the first release is not shown  
in this paper), and can continue to be used as a benchmark for future revisions.

## 6 Conclusions

In this paper, we have performed a ‘ground-to-space’ radiative closure study using the FINESSE instrument and an overpass  
415 of the PREFIRE satellite 1. To our knowledge, this is the first attempt at this type of experiment in the far-infrared. Thorough  
consideration of the various sources of uncertainty confirmed the validity of this approach and illustrated the main challenges  
in this experiment.

The ground-based FINESSE instrument demonstrated excellent closure, in particular when simulations used atmospheric  
data from the ERA5 reanalysis. Simulations based on in situ data did not agree as well with the FINESSE observations. This is  
420 a contrasting result to that found with FINESSE by Mosselmans et al. (2026), but may reflect the use of a different radiosonde  
brand in our study. The radiance results, and additional comparisons between ERA5 profiles and radiosonde launches through-  
out the WHAFFERS campaign, led us to conclude that there is likely a dry bias in humidity measurements from the iMet-4  
radiosonde in the very dry conditions of the campaign. The largest source of uncertainty in the comparison between simulated  
and observed radiances was in the specification of atmospheric water vapour profile, followed by the spectroscopy of water  
425 vapour. Many other authors note that precisely determining water vapour spectroscopy from field studies is limited by uncer-  
tainties in atmospheric water vapour content, and so we encourage further laboratory study and for future field studies targeting



the region to be designed with accurate, precise, and independent determination of water vapour at their core. These techniques will also help to calibrate and validate observations from the upcoming Far-infrared Outgoing Radiation Understanding and Monitoring (FORUM) satellite mission, scheduled to launch in 2028 (Palchetti et al., 2020).

430 The agreement of PREFIRE observations of upwelling radiances at the top-of-the-atmosphere with simulations varied by spectral region. In the mid-infrared and FIR dirty window, the agreement is only slightly weaker than obtained for the downwelling FINESSE measurements, though PREFIRE residual points are more scattered. In the furthest infrared band (185–330  $\text{cm}^{-1}$ ) agreement was somewhat poorer, largely due to a high radiometric noise in the PREFIRE TIRS instrument which may be underestimated at present. We also noted that inaccurate specification of water vapour by the radiosonde, diagnosed by  
435 FINESSE, degraded the PREFIRE residuals in the FIR dirty window, reinforcing the importance of water vapour profiling for these experiments. In these dry conditions, the infrared window and the FIR dirty window are both sensitive to the surface, and so uncertainty in our results was dominated by specification of surface temperature and emissivity in these spectral regions. We found that the use of independent satellite-observed surface temperature was able to remedy a bias in that from ERA5. However, it appears there remain some small systematic errors. Rigorous quantification of these errors will require further  
440 targeted comparisons over a longer time period and a wider range of conditions. We note that the approach developed here, and the database of simulated radiances with associated uncertainties will be useful for validating further efforts by the PREFIRE team to correct biases in the measured radiances. We discussed potential options for reducing the surface uncertainty, including the use of other field or satellite measurements.

PREFIRE, and the upcoming FORUM mission, open a new measurement window from space. They are designed to exploit  
445 the information content within the far-infrared to provide new insights into water vapour distributions, the radiative effects of clouds and, where conditions permit, surface properties. However, the community must be prepared with the right set of experimental designs and auxiliary measurement capabilities to comprehensively validate the new observations and hence maximise their scientific impact. Our study provides a stepping stone towards this goal.

*Data availability.* At time of submission, measurement data used in this study from the WHAFFFERS campaign are not yet available in an  
450 open archive, but can be accessed upon request to the authors.

*Author contributions.* BP and HB conceived the study. BP carried out the investigation and wrote the first draft of the manuscript, with supervision from HB and RH. JM, SM, SP, LW, YH, and BR-B took field measurements on the WHAFFFERS campaign. TL provided PREFIRE expertise and data curation. SM, SP, LW, and BR-B provided input to the radiative transfer modelling methodology. HO, DS, HB, and YH assisted with funding acquisition and project administration for the WHAFFFERS campaign. All authors assisted with editing the  
455 manuscript.

*Competing interests.* The authors declare that they have no conflict of interest.



460 *Acknowledgements.* The deployment of FINESSE on the WHAFFFERS campaign was supported by the European Space Agency (ESA) with grant number 4000137153/22/NL/IA. BP, SM, and SP were funded by the UK Natural Environment Research Council (NERC) via the SSCP DTP, grant number NE/S007415/1. HB and JM were supported by NERC under grant no. NE/Y006216/1. Field data were recorded at the Gault Nature Reserve of McGill University. For their contributions to the operation of the WHAFFFERS campaign we thank Lei Liu, Ruogu He, Mathieu Noreau, Eve Bigras, Veronique Meunier, and Calin Giurgiu from McGill University, and Jonathan Gero from University of Wisconsin-Madison. We would like to thank Aronne Merrelli, Nathaniel Miller, and Tim Michaels on the PREFIRE team for their assistance with data access and manuscript review.



## References

- 465 Agustí-Panareda, A., Diamantakis, M., Massart, S., Chevallier, F., Muñoz-Sabater, J., Barré, J., Curcoll, R., Engelen, R., Langerock, B., Law, R. M., Loh, Z., Morguí, J. A., Parrington, M., Peuch, V.-H., Ramonet, M., Roehl, C., Vermeulen, A. T., Warneke, T., and Wunch, D.: Modelling CO<sub>2</sub> weather – why horizontal resolution matters, *Atmospheric Chemistry and Physics*, 19, 7347–7376, <https://doi.org/10.5194/acp-19-7347-2019>, 2019.
- Bantges, R. J., Brindley, H. E., Murray, J. E., Last, A. E., Russell, J. E., Fox, C., Fox, S., Harlow, C., O’Shea, S. J., Bower, K. N., Baum, 470 B. A., Yang, P., Oetjen, H., and Pickering, J. C.: A test of the ability of current bulk optical models to represent the radiative properties of cirrus cloud across the mid- and far-infrared, *Atmospheric Chemistry and Physics*, 20, 12 889–12 903, <https://doi.org/10.5194/acp-20-12889-2020>, 2020.
- Baran, A. J.: The impact of cirrus microphysical and macrophysical properties on upwelling far-infrared spectra, *Quarterly Journal of the Royal Meteorological Society*, 133, 1425–1437, <https://doi.org/10.1002/qj.132>, [\\_eprint: https://rmets.onlinelibrary.wiley.com/doi/pdf/10.1002/qj.132](https://rmets.onlinelibrary.wiley.com/doi/pdf/10.1002/qj.132), 2007.
- 475 Bellisario, C., Brindley, H. E., Murray, J. E., Last, A., Pickering, J., Harlow, R. C., Fox, S., Fox, C., Newman, S. M., Smith, M., Anderson, D., Huang, X., and Chen, X.: Retrievals of the Far Infrared Surface Emissivity Over the Greenland Plateau Using the Tropospheric Airborne Fourier Transform Spectrometer (TAFTS), *Journal of Geophysical Research: Atmospheres*, 122, <https://doi.org/10.1002/2017JD027328>, 2017.
- 480 Belotti, C., Barbara, F., Barucci, M., Bianchini, G., D’Amato, F., Del Bianco, S., Di Natale, G., Gai, M., Montori, A., Pratesi, F., Rettinger, M., Rolf, C., Sussmann, R., Trickl, T., Viciani, S., Vogelmann, H., and Palchetti, L.: The Far-Infrared Radiation Mobile Observation System (FIRMOS) for spectral characterization of the atmospheric emission, *Atmospheric Measurement Techniques*, 16, 2511–2529, <https://doi.org/10.5194/amt-16-2511-2023>, 2023.
- Brindley, H. E. and Harries, J. E.: The impact of far i.r. absorption on clear sky greenhouse forcing: sensitivity studies at high spectral 485 resolution, *Journal of Quantitative Spectroscopy and Radiative Transfer*, 60, 151–180, [https://doi.org/10.1016/S0022-4073\(97\)00152-0](https://doi.org/10.1016/S0022-4073(97)00152-0), 1998.
- Bullister, J. L. and Warner, M. J.: Atmospheric Histories (1765-2022) for CFC-11, CFC-12, CFC-113, CCl<sub>4</sub>, SF<sub>6</sub> and N<sub>2</sub>O (NCEI Accession 0164584), [https://doi.org/10.3334/CDIAC/OTG.CFC\\_ATM\\_HIST\\_2015](https://doi.org/10.3334/CDIAC/OTG.CFC_ATM_HIST_2015), 2017.
- Chen, X., Huang, X., and Flanner, M. G.: Sensitivity of modeled far-IR radiation budgets in polar continents to treatments of snow surface 490 and ice cloud radiative properties, *Geophysical Research Letters*, 41, 6530–6537, <https://doi.org/10.1002/2014GL061216>, 2014.
- Clough, S. A., Shephard, M. W., Mlawer, E. J., Delamere, J. S., Iacono, M. J., Cady-Pereira, K., Boukabara, S., and Brown, P. D.: Atmospheric radiative transfer modeling: a summary of the AER codes, *Journal of Quantitative Spectroscopy and Radiative Transfer*, 91, 233–244, <https://doi.org/10.1016/j.jqsrt.2004.05.058>, 2005.
- Delamere, J. S., Clough, S. A., Payne, V. H., Mlawer, E. J., Turner, D. D., and Gamache, R. R.: A far-infrared radiative closure study in the Arctic: Application to water vapor, *Journal of Geophysical Research: Atmospheres*, 115, 2009JD012968, 495 <https://doi.org/10.1029/2009JD012968>, 2010.
- Di Natale, G., Brindley, H., Warwick, L., Panditharatne, S., Yang, P., David, R. O., Carlsen, T., Vâjâiac, S. N., Vlad, A., Ghemulet, S., Bantges, R., Foth, A., Flügge, M., Lyngra, R., Oetjen, H., Schuettmeyer, D., Palchetti, L., and Murray, J.: Achieving consistency between in-situ and remotely sensed optical and microphysical properties of Arctic cirrus: the impact of far-infrared radiances, *Atmospheric 500 Chemistry and Physics*, 26, 1373–1394, <https://doi.org/10.5194/acp-26-1373-2026>, 2026.



- Drouin, B. J., L'Ecuyer, T., Padmanabhan, S., Foote, M., Bendig, R., Calcutt, S., Hawkins, G., Herzog, H., Hochberg, E., Kenyon, M., Mariani, G., Martinez, D. A., McGuire, J., Mckinley, I., Merrelli, A., Nemchick, D., Raouf, N., Spiers, G., and Wilson, D.: Thermal Infrared Spectrometers for the Polar Radiant Energy in the Far-Infrared Experiment (PREFIRE), *Earth and Space Science*, 12, e2024EA003711, <https://doi.org/10.1029/2024EA003711>, 2025.
- 505 Dzambo, A. M., Turner, D. D., and Mlawer, E. J.: Evaluation of two Vaisala RS92 radiosonde solar radiative dry bias correction algorithms, *Atmospheric Measurement Techniques*, 9, 1613–1626, <https://doi.org/10.5194/amt-9-1613-2016>, 2016.
- Feldman, D. R., Liou, K. N., Shia, R. L., and Yung, Y. L.: On the information content of the thermal infrared cooling rate profile from satellite instrument measurements, *Journal of Geophysical Research: Atmospheres*, 113, 2007JD009041, <https://doi.org/10.1029/2007JD009041>, 2008.
- 510 Fischer, L., Craig, G. C., and Kiemle, C.: Horizontal structure function and vertical correlation analysis of mesoscale water vapor variability observed by airborne lidar, *Journal of Geophysical Research: Atmospheres*, 118, 7579–7590, <https://doi.org/10.1002/jgrd.50588>, 2013.
- Flores, F., Rondanelli, R., Díaz, M., Querel, R., Mundnich, K., Herrera, L. A., Pola, D., and Carricajo, T.: The Life Cycle of a Radiosonde, *Bulletin of the American Meteorological Society*, 94, 187–198, <https://doi.org/10.1175/BAMS-D-11-00163.1>, 2013.
- Ghysels, M., Durry, G., Amarouche, N., Hurst, D., Hall, E., Xiong, K., Dupont, J.-C., Samake, J.-C., Frérot, F., Bejjani, R., and Riviere, E. D.: Pico-Light H<sub>2</sub>O: intercomparison of in situ water vapour measurements during the AsA 2022 campaign, *Atmospheric Measurement Techniques*, 17, 3495–3513, <https://doi.org/10.5194/amt-17-3495-2024>, 2024.
- 515 Hanel, R. A., Schlachman, B., Rogers, D., and Vanous, D.: Nimbus 4 Michelson Interferometer, *Applied Optics*, 10, 1376, <https://doi.org/10.1364/AO.10.001376>, 1971.
- Harries, J., Carli, B., Rizzi, R., Serio, C., Mlynyczak, M., Palchetti, L., Maestri, T., Brindley, H., and Masiello, G.: The Far-infrared Earth, *Reviews of Geophysics*, 46, <https://doi.org/10.1029/2007RG000233>, [https://doi.org/https://doi.org/10.1029/2007RG000233](https://agupubs.onlinelibrary.wiley.com/doi/pdf/10.1029/2007RG000233), [\\_eprint: https://agupubs.onlinelibrary.wiley.com/doi/pdf/10.1029/2007RG000233](https://agupubs.onlinelibrary.wiley.com/doi/pdf/10.1029/2007RG000233), 2008.
- 520 Hersbach, H., Bell, B., Berrisford, P., Hirahara, S., Horányi, A., Muñoz-Sabater, J., Nicolas, J., Peubey, C., Radu, R., Schepers, D., Simons, A., Soci, C., Abdalla, S., Abellan, X., Balsamo, G., Bechtold, P., Biavati, G., Bidlot, J., Bonavita, M., De Chiara, G., Dahlgren, P., Dee, D., Diamantakis, M., Dragani, R., Flemming, J., Forbes, R., Fuentes, M., Geer, A., Haimberger, L., Healy, S., Hogan, R. J., Hólm, E., Janisková, M., Keeley, S., Laloyaux, P., Lopez, P., Lupu, C., Radnoti, G., de Rosnay, P., Rozum, I., Vamborg, F., Villaume, S., and Thépaut, J.-N.: The ERA5 global reanalysis, *Quarterly Journal of the Royal Meteorological Society*, 146, 1999–2049, <https://doi.org/https://doi.org/10.1002/qj.3803>, [\\_eprint: https://rmets.onlinelibrary.wiley.com/doi/pdf/10.1002/qj.3803](https://doi.org/https://doi.org/10.1002/qj.3803), 2020.
- 525 Hogan, R. J. and Matricardi, M.: Evaluating and improving the treatment of gases in radiation schemes: the Correlated K-Distribution Model Intercomparison Project (CKDMIP), *Geoscientific Model Development*, 13, 6501–6521, <https://doi.org/10.5194/gmd-13-6501-2020>, 2020.
- 530 Hokanson Wagner, E., Drouin, B., Michaels, T., and Merrelli, A.: PREFIRE Data User Guide: Level 1B Radiance (1B-RAD), Tech. rep., [https://asdc.larc.nasa.gov/documents/prefire/guide/PREFIRE\\_Data\\_User\\_Guide\\_1B-RAD\\_R01-20250430.pdf](https://asdc.larc.nasa.gov/documents/prefire/guide/PREFIRE_Data_User_Guide_1B-RAD_R01-20250430.pdf), version R01, 2025.
- Huang, X., Chen, X., Zhou, D. K., and Liu, X.: An Observationally Based Global Band-by-Band Surface Emissivity Dataset for Climate and Weather Simulations, *Journal of the Atmospheric Sciences*, 73, 3541 – 3555, <https://doi.org/10.1175/JAS-D-15-0355.1>, place: Boston MA, USA, 2016.
- 535 Huang, X., Chen, X., Flanner, M., Yang, P., Feldman, D., and Kuo, C.: Improved Representation of Surface Spectral Emissivity in a Global Climate Model and Its Impact on Simulated Climate, *Journal of Climate*, 31, 3711–3727, <https://doi.org/10.1175/JCLI-D-17-0125.1>, 2018.



- Hurst, D. F., Hall, E. G., Jordan, A. F., Miloshevich, L. M., Whiteman, D. N., Leblanc, T., Walsh, D., Vömel, H., and Oltmans, S. J.: Comparisons of temperature, pressure and humidity measurements by balloon-borne radiosondes and frost point hygrometers during MOHAVE-2009, *Atmospheric Measurement Techniques*, 4, 2777–2793, <https://doi.org/10.5194/amt-4-2777-2011>, 2011.
- InterMet Systems: iMet-4 Radiosonde Technical Data Sheet, Tech. rep., InterMet Systems, Grand Rapids, MI, USA, [https://www.intermetystems.com/wp-content/uploads/2022/01/202084-12\\_iMet-4\\_Technical\\_Data\\_Sheet.pdf](https://www.intermetystems.com/wp-content/uploads/2022/01/202084-12_iMet-4_Technical_Data_Sheet.pdf), 2022.
- Kempe, V., Oertel, D., Schuster, R., Becker-Ross, H., and Jahn, H.: Absolute IR-spectra from the measurement of Fourier-spectrometers aboard Meteor 25 and 28, *Acta Astronautica*, 7, 1403–1416, [https://doi.org/10.1016/0094-5765\(80\)90015-6](https://doi.org/10.1016/0094-5765(80)90015-6), 1980.
- Liu, L., Bliankinshtein, N., Huang, Y., Gyakum, J. R., Gabriel, P. M., Xu, S., and Wolde, M.: Radiative closure tests of collocated hyperspectral microwave and infrared radiometers, *Atmospheric Measurement Techniques*, 17, 2219–2233, <https://doi.org/10.5194/amt-17-2219-2024>, 2024.
- L’Ecuyer, T. S., Drouin, B. J., Anheuser, J., Grames, M., Henderson, D. S., Huang, X., Kahn, B. H., Kay, J. E., Lim, B. H., Mateling, M., Merrelli, A., Miller, N. B., Padmanabhan, S., Peterson, C., Schlegel, N.-J., White, M. L., and Xie, Y.: The Polar Radiant Energy in the Far Infrared Experiment: A New Perspective on Polar Longwave Energy Exchanges, *Bulletin of the American Meteorological Society*, 102, E1431 – E1449, <https://doi.org/10.1175/BAMS-D-20-0155.1>, place: Boston MA, USA, 2021.
- Maestri, T., Rizzi, R., Tosi, E., Veglio, P., Palchetti, L., Bianchini, G., Di Girolamo, P., Masiello, G., Serio, C., and Summa, D.: Analysis of cirrus cloud spectral signatures in the far infrared, *Journal of Quantitative Spectroscopy and Radiative Transfer*, 141, 49–64, <https://doi.org/10.1016/j.jqsrt.2014.02.030>, 2014.
- Mariani, Z., Strong, K., Wolff, M., Rowe, P., Walden, V., Fogal, P. F., Duck, T., Lesins, G., Turner, D. S., Cox, C., Eloranta, E., Drummond, J. R., Roy, C., Turner, D. D., Hudak, D., and Lindenmaier, I. A.: Infrared measurements in the Arctic using two Atmospheric Emitted Radiance Interferometers, *Atmospheric Measurement Techniques*, 5, 329–344, <https://doi.org/10.5194/amt-5-329-2012>, 2012.
- Mattingly, K., Hokanson Wagner, E., Michaels, T., and Merrelli, A.: PREFIRE Data User Guide Auxiliary Meteorology (AUX-MET), Tech. rep., [https://asdc.larc.nasa.gov/documents/prefire/guide/PREFIRE\\_Data\\_User\\_Guide\\_AUX-MET\\_R01.pdf](https://asdc.larc.nasa.gov/documents/prefire/guide/PREFIRE_Data_User_Guide_AUX-MET_R01.pdf), version R01, 2025.
- Miloshevich, L. M., Vömel, H., Whiteman, D. N., and Leblanc, T.: Accuracy assessment and correction of Vaisala RS92 radiosonde water vapor measurements, *Journal of Geophysical Research: Atmospheres*, 114, 2008JD011565, <https://doi.org/10.1029/2008JD011565>, 2009.
- Mlawer, E. J., Turner, D. D., Paine, S. N., Palchetti, L., Bianchini, G., Payne, V. H., Cady-Pereira, K. E., Pernak, R. L., Alvarado, M. J., Gombos, D., Delamere, J. S., Mlynczak, M. G., and Mast, J. C.: Analysis of Water Vapor Absorption in the Far-Infrared and Submillimeter Regions Using Surface Radiometric Measurements From Extremely Dry Locations, *Journal of Geophysical Research: Atmospheres*, 124, 8134–8160, <https://doi.org/10.1029/2018JD029508>, 2019.
- Mlawer, E. J., Cady-Pereira, K. E., Mascio, J., and Gordon, I. E.: The inclusion of the MT\_CKD water vapor continuum model in the HITRAN molecular spectroscopic database, *Journal of Quantitative Spectroscopy and Radiative Transfer*, 306, 108645, <https://doi.org/https://doi.org/10.1016/j.jqsrt.2023.108645>, 2023.
- Mosselmans, S., Elizabeth Brindley, H., Cox, C., Gryspeerd, E., Murray, J., Panditharatne, S., Warwick, L., Schuettmeyer, D., Oetjen, H., Carlsen, T., Foth, A., and David, R.: Exploring Clear-Sky Longwave Radiative Closure in the Arctic: A Downwelling Case Study, *Atmospheric Science Letters*, 27, e70000, <https://doi.org/10.1002/asl.70000>, 2026.
- Murray, J. E., Brindley, H. E., Fox, S., Bellisario, C., Pickering, J. C., Fox, C., Harlow, C., Smith, M., Anderson, D., Huang, X., Chen, X., Last, A., and Bantges, R.: Retrievals of High-Latitude Surface Emissivity Across the Infrared From High-Altitude Aircraft Flights, *Journal of Geophysical Research: Atmospheres*, 125, e2020JD033672, <https://doi.org/10.1029/2020JD033672>, 2020.



- 575 Murray, J. E., Warwick, L., Brindley, H., Last, A., Quigley, P., Rochester, A., Dewar, A., and Cummins, D.: The Far-INfrarEd Spectrometer for Surface Emissivity (FINESSE) – Part 1: Instrument description and level 1 radiances, *Atmospheric Measurement Techniques*, 17, 4757–4775, <https://doi.org/10.5194/amt-17-4757-2024>, 2024.
- NOAA: Global Monitoring Laboratory: Carbon Cycle Greenhouse Gases, <https://gml.noaa.gov/ccgg/data/>.
- Oreopoulos, L., Mlawer, E., Delamere, J., Shippert, T., Cole, J., Fomin, B., Iacono, M., Jin, Z., Li, J., Manners, J., Räisänen, P., Rose, 580 F., Zhang, Y., Wilson, M. J., and Rossow, W. B.: The Continual Intercomparison of Radiation Codes: Results from Phase I, *Journal of Geophysical Research: Atmospheres*, 117, 2011JD016821, <https://doi.org/10.1029/2011JD016821>, 2012.
- Palchetti, L., Brindley, H., Bantges, R., Buehler, S. A., Camy-Peyret, C., Carli, B., Cortesi, U., Del Bianco, S., Di Natale, G., Dinelli, B. M., Feldman, D., Huang, X. L., C.-Labonnote, L., Libois, Q., Maestri, T., Mlynzack, M. G., Murray, J. E., Oetjen, H., Ridolfi, M., Riese, M., Russell, J., Saunders, R., and Serio, C.: FORUM: Unique Far-Infrared Satellite Observations to Better Understand How Earth Radiates 585 Energy to Space, *Bulletin of the American Meteorological Society*, 101, E2030–E2046, <https://doi.org/10.1175/BAMS-D-19-0322.1>, 2020.
- Panditharatne, S., Cox, C., Song, R., Siddans, R., Bantges, R., Murray, J., Fox, S., Fox, C., and Brindley, H.: Exploiting airborne far-infrared measurements to optimise an ice cloud retrieval, *Atmospheric Chemistry and Physics*, 25, 9981–9998, <https://doi.org/10.5194/acp-25-9981-2025>, 2025.
- 590 PREFIRE team: PREFIRE Spectral Response Function, <https://prefire.ssec.wisc.edu/SRF/>, 2025.
- Ridolfi, M., Tirelli, C., Ceccherini, S., Belotti, C., Cortesi, U., and Palchetti, L.: Synergistic retrieval and complete data fusion methods applied to simulated FORUM and IASI-NG measurements, *Atmospheric Measurement Techniques*, 15, 6723–6737, <https://doi.org/10.5194/amt-15-6723-2022>, 2022.
- Rodgers, C. D.: Inverse Methods for Atmospheric Sounding: Theory and Practice, vol. 2 of *Series on Atmospheric, Oceanic and Planetary Physics*, WORLD SCIENTIFIC, ISBN 978-981-02-2740-1 978-981-281-371-8, <https://doi.org/10.1142/3171>, 2000.
- 595 Rowe, P. M., Miloshevich, L. M., Turner, D. D., and Walden, V. P.: Dry Bias in Vaisala RS90 Radiosonde Humidity Profiles over Antarctica, *Journal of Atmospheric and Oceanic Technology*, 25, 1529–1541, <https://doi.org/10.1175/2008JTECHA1009.1>, 2008.
- Sinha, A. and Harries, J. E.: Water vapour and greenhouse trapping: The role of far infrared absorption, *Geophysical Research Letters*, 22, 2147–2150, <https://doi.org/10.1029/95GL01891>, 1995.
- 600 Sussmann, R., Reichert, A., and Rettinger, M.: The Zugspitze radiative closure experiment for quantifying water vapor absorption over the terrestrial and solar infrared –Part 1: Setup, uncertainty analysis, and assessment of far-infrared watervapor continuum, *Atmospheric Chemistry and Physics*, 16, 11649–11669, <https://doi.org/10.5194/acp-16-11649-2016>, 2016.
- Turner, D. D., Merrelli, A., Vimont, D., and Mlawer, E. J.: Impact of modifying the longwave water vapor continuum absorption model on community Earth system model simulations, *Journal of Geophysical Research: Atmospheres*, 117, 2011JD016440, 605 <https://doi.org/10.1029/2011JD016440>, 2012.
- Vaisala: HMP155 User Guide, Tech. rep., Vaisala, Vantaa, Finland, <https://docs.vaisala.com/r/M210912EN-J/en-US>, 2025.
- Vömel, H., Selkirk, H., Miloshevich, L., Valverde-Canossa, J., Valdés, J., Kyrö, E., Kivi, R., Stolz, W., Peng, G., and Diaz, J. A.: Radiation Dry Bias of the Vaisala RS92 Humidity Sensor, *Journal of Atmospheric and Oceanic Technology*, 24, 953–963, <https://doi.org/10.1175/JTECH2019.1>, 2007.
- 610 Wang, S., Ren, T., Yang, P., Saito, M., and Brindley, H. E.: Improved Temperature-Dependent Ice Refractive Index Compilation in the Far-Infrared Spectrum, *Geophysical Research Letters*, 51, e2024GL110176, <https://doi.org/10.1029/2024GL110176>, <https://agupubs.onlinelibrary.wiley.com/doi/pdf/10.1029/2024GL110176>, 2024.



- Warwick, L., Brindley, H., Di Roma, A., Fox, S., Havemann, S., Murray, J., Oetjen, H., Price, H. C., Schüttemeyer, D., Sgheri, L., and Tideman, D. A.: Retrieval of Tropospheric Water Vapor From Airborne Far-Infrared Measurements: A Case Study, *Journal of Geophysical Research: Atmospheres*, 127, e2020JD034 229, <https://doi.org/10.1029/2020JD034229>, 2022.
- 615
- Warwick, L., Murray, J. E., and Brindley, H.: The Far-INfrarEd Spectrometer for Surface Emissivity (FINESSE) – Part 2: First measurements of the emissivity of water in the far-infrared, *Atmospheric Measurement Techniques*, 17, 4777–4787, <https://doi.org/10.5194/amt-17-4777-2024>, 2024.
- Warwick, L., Oetjen, H., Murray, J., Panditharatne, S., Brindley, H., Schuettemeyer, D., Chen, X., and Huang, X.: In Situ Measurements of Ice and Snow Emissivity in the Far-Infrared, *Earth and Space Science*, 12, e2025EA004 350, <https://doi.org/10.1029/2025EA004350>, 2025.
- 620
- Yang, P., Mlynczak, M. G., Wei, H., Kratz, D. P., Baum, B. A., Hu, Y. X., Wiscombe, W. J., Heidinger, A., and Mishchenko, M. I.: Spectral signature of ice clouds in the far-infrared region: Single-scattering calculations and radiative sensitivity study, *Journal of Geophysical Research: Atmospheres*, 108, <https://doi.org/https://doi.org/10.1029/2002JD003291>, <https://agupubs.onlinelibrary.wiley.com/doi/pdf/10.1029/2002JD003291>, 2003.
- 625